Chapter 2 (Part I)

Rechargeable aqueous aluminum-metal battery with exfoliated graphite as cathode

Nandi, S., Das S. K. *ACS Sustainable Chem. Eng.* 7:19839-19847, 2019.

Rechargeable aqueous aluminum-metal battery with exfoliated graphite as cathode

2.1.1 Introduction

As mentioned in the introduction chapter, rechargeable aluminum (Al) batteries are a new entrant to the family of rechargeable batteries. A recent yet exemplary example is the chloroaluminate electrolyte-based Al-metal battery with a carbonaceous cathode [1-7]. Most of the works on Al-metal or ion batteries use chloroaluminate-based ionic liquid electrolytes such as $AlCl_3$/[EMIM]Cl [1-12]. This is because reversible electrodeposition of Al on Al is found to be possible in chloroaluminate electrolytes [13-14]. Although the electrochemical stability of chloroaluminate electrolytes spans over a wide potential window (~ 2.4 V), the difficulty in handling them in air and their extreme corrosive nature coupled with an exorbitant cost may certainly be a deterrent in achieving safe and low-cost Al-metal/ion batteries. These demerits cast a pall over the greater promise of chloroaluminate electrolyte-based Al-metal/ion batteries. Nevertheless, this is a starting point to think beyond chloroaluminate electrolyte and a potential alternative is to use water-based (or aqueous) electrolyte. The aqueous electrolytes offer several distinct advantages such as high ionic conductivity and high dissociation of ionic salts besides lowering the cost and safety of the battery [15-17]. Therefore, there are fine examples of both aqueous Al-metal and Al-ion batteries [18-27]. Conventional belief advises against direct use of Al metal in aqueous electrolyte due to hydrogen evolution [28-30]. However, Zhao et al. recently suggested a possibility of directly using Al metal in a rechargeable aqueous system by creating a solid electrolyte interphase on Al surface, again by treating the Al electrode in chloroaluminate electrolyte [26]. When coupled with MnO_2 cathode, the aqueous Al-metal battery demonstrated a discharge capacity of 168 $mAhg^{-1}$ at the end of 40^{th} cycle at a current rate of 100 mAg^{-1} in 2 molar $Al(CF_3SO_3)_3$ aqueous electrolyte.

In this chapter, the electrochemical performance of an aqueous Al-metal battery is illustrated with graphite cathode. The graphite electrode was pretreated using a simple electrochemical method. The pretreatment process changes the surface morphology of the graphite electrode and results in formation of graphite flakes, which is later termed as exfoliated graphite foam.

2.1.2 Experimental Section

2.1.2.1 Materials

Metallic Aluminum (Al) foil (Brand name: Hindalco Freshwrapp) was obtained from local grocery store (Figure 2.1.1a). This type of Al foil is generally used for household purposes such as for wrapping food items. Graphite foil was obtained from Nikunz Exim Pvt Ltd. Aluminum chloride hexahydrate ($AlCl_3.6H_2O$) is used as the ionic salt for preparing the electrolyte. Aluminum hydroxide ($Al(OH)_3$) was obtained from Loba Chemie (CAS # 21645-51-2).

2.1.2.2 Electrochemical exfoliation

Pretreatment of Al and graphite: The pretreatment process is electrochemically performed with two different counter electrodes namely Al and Copper (Cu) foils. A note of caution is that one should be extremely careful while mixing $AlCl_3$ in water since the reaction is exothermic.

(i) Firstly, with Al counter electrode: An Al-graphite cell is first assembled by dipping a metallic Al electrode (breadth = 1 cm and length = 1.5 cm) and graphite electrode (breadth = 1 cm and length = 1.5 cm) in 1 M $AlCl_3$ aqueous electrolyte in a glass cell. The separation between the Al and graphite electrodes is 1 cm. The immersion length of both the electrodes in the electrolyte is 1 cm. A dc potential (or bias) of 1 V, 2.5 V and 4 V is separately applied between the electrodes of different Al-graphite cells using a DC power source for 5 min. The positive (cathode) and negative (anode) terminals of the power supply are connected to graphite and Al respectively. The experimental set-up is shown in Figure 2.1.1 (b, c). Experiments were also performed with different bias time. There were formations of vigorous air bubbles in both the electrodes. Expansion of the graphite foil could be observed, which are later called as exfoliated graphite electrode. These pretreated Al-graphite cells were directly used for further electrochemical investigations. In this case, hence, note that both the Al and graphite electrodes are pretreated simultaneously.

(ii) Secondly, with Cu counter electrode: Instead of Al, now Cu is used for assembling Cu-graphite cell in 1 M $AlCl_3$ aqueous electrolyte in a glass cell. The dimensions and all other conditions are identical to the previous case of Al-graphite cell. A dc potential (or bias) of 3 V is applied between the electrodes of Cu-graphite cell for 5

min. A large expansion of the graphite electrode took place. This exfoliated graphite foil is separated out from the Cu-graphite cell and it is used for further electrochemical experiments with Al. Basically, this exfoliated graphite foil is paired with a pretreated Al (separated out from an Al-graphite cell which was pretreated at a bias of 4 V for 5 min) to obtain new pretreated Al-graphite cell.

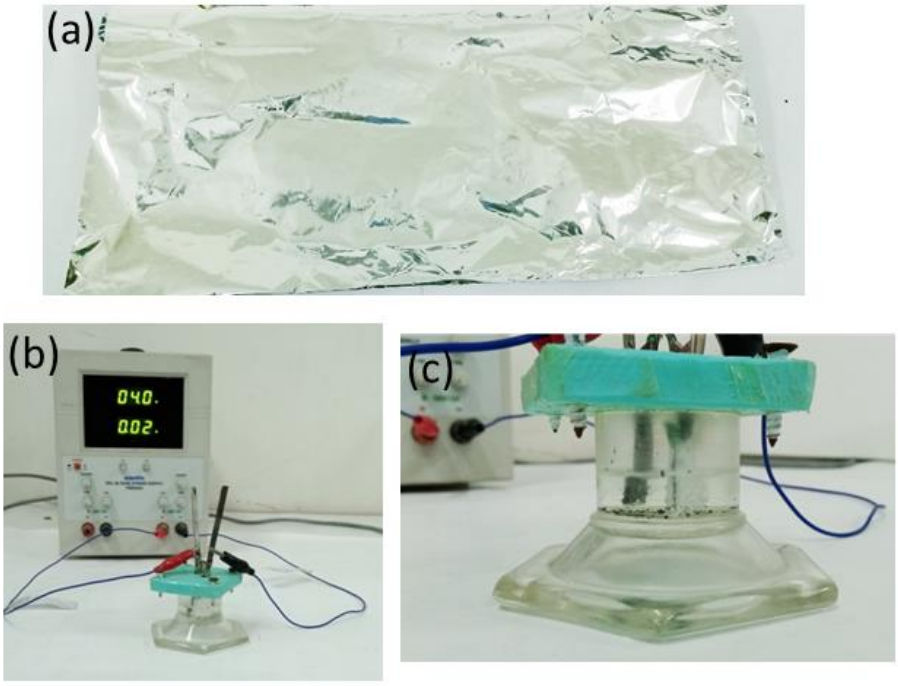

Figure 2.1.1 (a) Digital photograph of Al foil used in the present work, (b) Experimental set up for performing the electrochemical exfoliation of graphite foil, and (c) enlarged view of the cell.

2.1.2.3 Characterization

The crystallographic phase identification was performed by using powder X-ray diffraction (BRUKER AXS D8 FOCUS; Cu-Kα radiation, λ = 1.5406 Å). The morphology was observed by scanning electron microscopy (SEM, JEOL JSM 6390LV) and transmission electron microscopy (TEM, JOEL JEM 2100). The chemical analysis measurements were recorded using X-ray photoelectron spectroscopy (XPS) and Raman spectroscopy with Physical Electronics (PHI 5000 Versa Probe III) and ENWAVE optronics (EZRaman-N).

2.1.2.4 Electrochemical analysis

Cyclic voltammetry (CV) and galvanostatic discharge/charge experiments were performed for certain combinations of Al and graphite electrodes which makes the Al-

graphite cells. The utilized electrolyte was 1 M $AlCl_3$ aqueous solution unless otherwise explicitly stated. The discharge/charge and CV experiments were performed in the voltage range of 0 V to 2 V. The scan rate for CV experiment was 1 mVs^{-1}. Electrochemical impedance spectra (EIS) were recorded for the following cells in the frequency range of 1 mHz-200 kHz at signal amplitude of 10 mV: (i) symmetric Al (pristine)-Al (pristine) cell, (ii) symmetric Al (pretreated)-Al (pretreated) cell, (iii) Al (pristine)-graphite (pristine) cell, (iv) Al (pretreated)-graphite (pretreated with Al) cell, and (v) Al (pretreated)-graphite (pretreated with Cu) cell.

CV experiments were also performed in a conventional three-electrode electrochemical glass cell and a symmetric Al-Al cell to observe any reversible electrodeposition of Al on Al in 1 M $AlCl_3$ aqueous electrolyte. Pt electrode and aqueous Ag/AgCl electrode were used as the counter and reference electrodes respectively for three electrode measurement. The voltage ranges were -1.8 V to -0.5 V and -0.5 V to 0.5 V for the three electrode and symmetric Al-Al cells respectively. All the electrochemical experiments were conducted at room temperature (25 ^oC) and at ambient atmosphere. For ex-situ XRD, SEM and XPS measurements, the electrodes were harvested after required discharge/charge cycles and dried at 110 ^oC for 24 h.

2.1.3 Results and Discussion

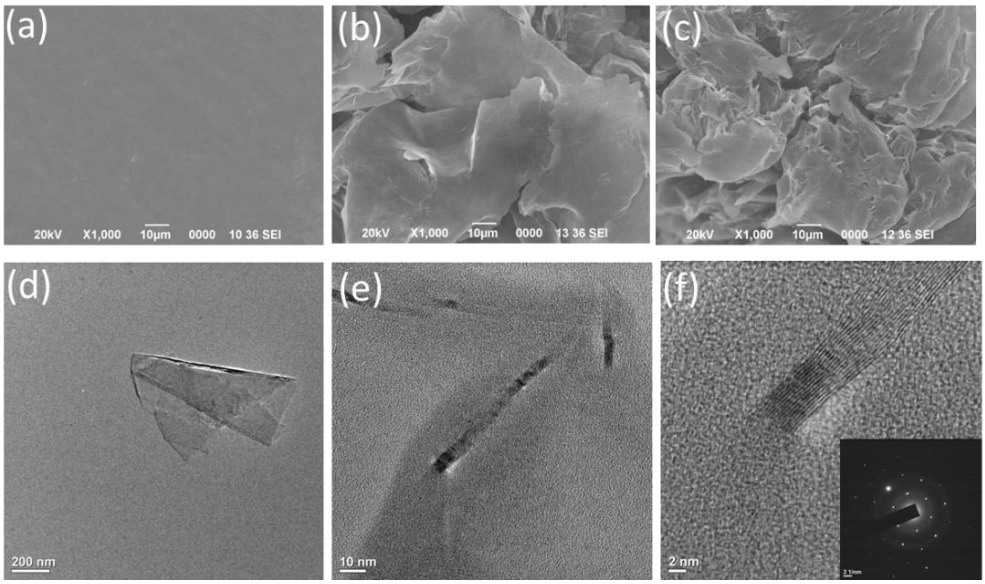

Figure 2.1.2 SEM images of (a) pristine graphite foil, (b) exfoliated graphite foil (or foam) with Al and (c) exfoliated graphite foil (or foam) with Cu. (d-f) TEM images of exfoliated graphite foil (or foam) with Cu. Inset of Figure 2.1.2f shows the SAED pattern.

Figure 2.1.2 (a-c) shows the SEM images of pristine graphite and electrochemically exfoliated graphite foam with Al and Cu as one of the counter electrodes in 1 M $AlCl_3$ aqueous electrolyte. It could be noticed that the surface of the exfoliated graphite foam is covered with nanoflakes (Figure 2.1.2b and 2.1.2c). TEM images, as shown in Figure 2.1.2 (d-f) of the exfoliated graphite foam again confirmed the formation of graphite nanoflakes. The graphitic layers could also be seen (Figure 2.1.2f). The SAED pattern (inset of Figure 2.1.2f) confirms the crystallinity of the nanoflakes. The XRD patterns (Figure 2.1.3a) also show retention of the graphitic structure. It is noted that expansion of the graphite foil with Cu counter electrode is quite larger than Al counter electrode despite using lower bias potential (i.e. 3 V for Cu and 4 V for Al). The digital photographs (Figure 2.1.3(c-e)) show the comparison of pristine graphite and exfoliated graphite foils. The thicknesses of the exfoliated graphite foils (or foams) are respectively 1.74 mm when biased with Cu (Figure 2.1.3h) and 0.74 (Figure 2.1.3g) mm when biased with Al, whereas pristine graphite thickness is 0.50 mm (Figure 2.1.3f).

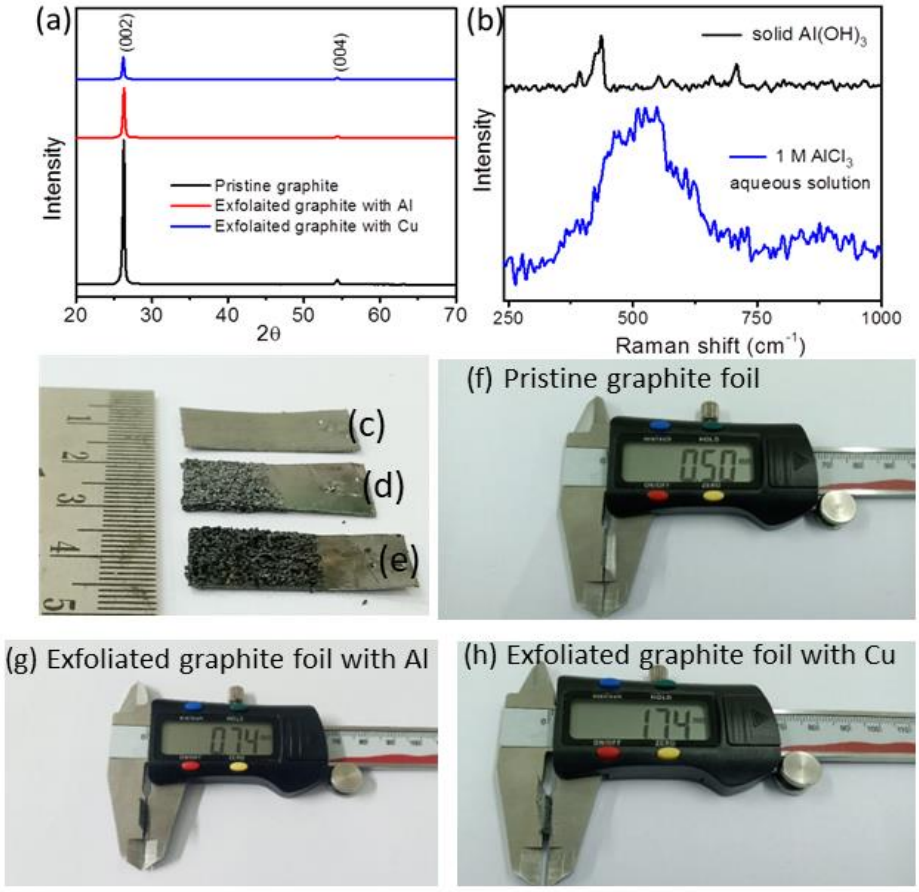

Figure 2.1.3 (a) XRD patterns of all graphite foils and (b) Raman spectra of 1 M aqueous solution of $AlCl_3.6H_2O$ and solid sample of $Al(OH)_3$. Digital photographs

and thickness measurement of (c-f) pristine graphite, (d-g) exfoliated graphite with Al and (e-h) exfoliated graphite with Cu.

A short note on the electrolyte: generally, it is believed that $AlCl_3$ hydrolyzes to $Al(OH)_3$. It is noted here that we did not observe any precipitation while preparing the electrolyte (Figure 2.1.4). The comparison of Raman spectra (Figure 2.1.3b) of 1 M aqueous solution of $AlCl_3.6H_2O$ and solid sample of $Al(OH)_3$ clearly shows the differences. The Raman peak around 525 cm^{-1} is attributed to $[Al(H_2O)_6]^{3+}$cation [31], which suggests that each Al^{3+} ion is hydrated by six H_2O molecules. Therefore, the possible charged species in the electrolyte are hydrated Al^{3+} cation and Cl^- anion.

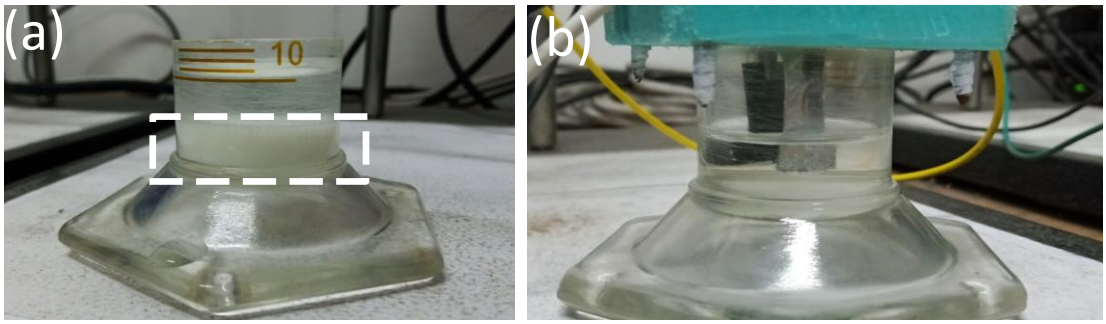

Figure 2.1.4 Digital photographs of (a) 300 mg of $Al(OH)_3$ in water solution and (b) 1 M aqueous solution of $AlCl_3.6H_2O$. The dotted line indicates that $Al(OH)_3$ is not soluble in water.

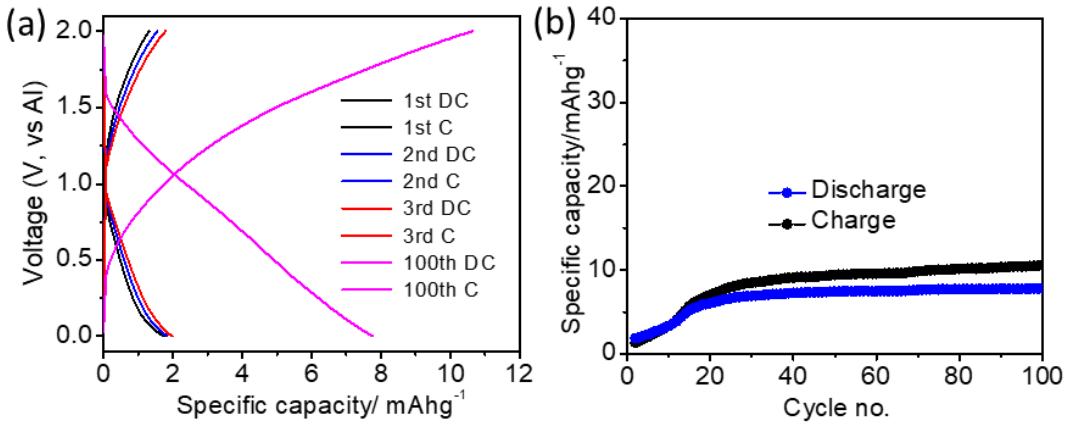

Figure 2.1.5 (a) Galvanostatic discharge/charge curves of pristine Al-graphite cell, (b) Variation of discharge/charge capacities with cycle number at a specific current density of 0.5 Ag^{-1} in 1 M $AlCl_3$ aqueous electrolyte.

Galvanostatic discharge/charge experiment was pursued initially with pristine Al and pristine graphite foil (both of them as available from market) in 1 M $AlCl_3$ aqueous electrolyte in the voltage range of 0-2 V (vs. Al) at current density of 0.5 Ag^{-}

[1]. As shown in Figure 2.1.5, the Al-graphite cell exhibits very low specific capacity (< 8 $mAhg^{-1}$). It is well-known in recent times that few-layer graphene foam delivers high discharge capacity (~ 60-110 $mAhg^{-1}$) in chloroaluminate electrolyte-based Al-metal battery [1, 3]. Hence, motivated by this very idea of using graphene foam in the aqueous Al-metal battery in an effort to improve the discharge capacity. The graphene foam electrodes were obtained by the electrochemical exfoliation of the graphite film as discussed in the experimental section.

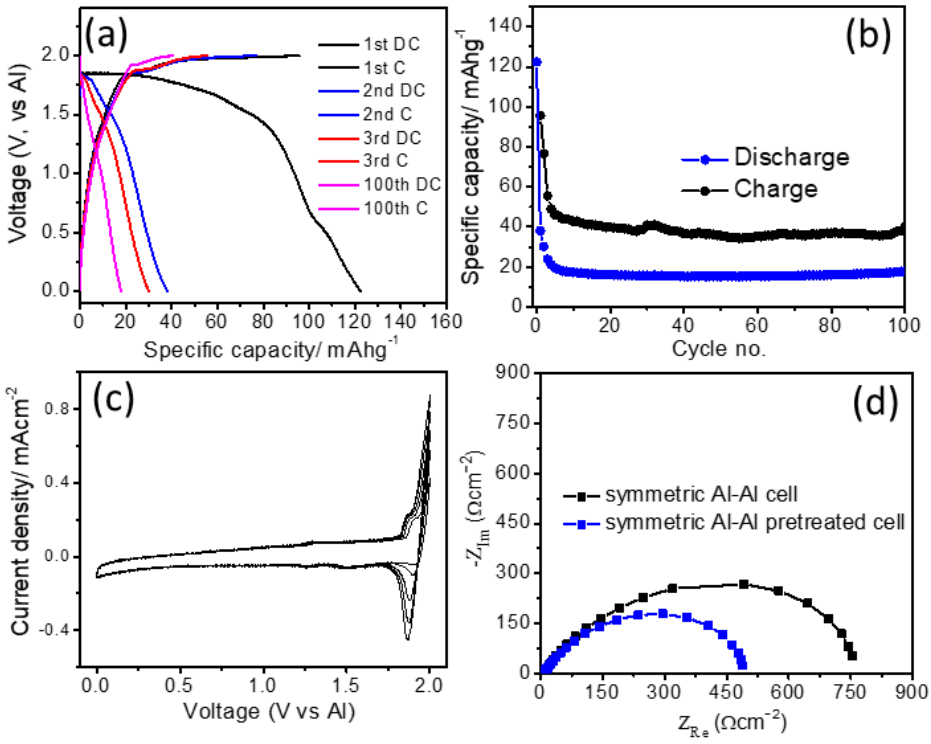

Figure 2.1.6 (a) Galvanostatic discharge/charge curves of pretreated Al-graphite foam cell (with bias of 4 V), (b) Variation of discharge/charge capacities with cycle number. The current density is 0.5 Ag^{-1}. (c) CV curves of Al-graphite foam cell (with bias of 4 V) at scan rate of 1 mVs^{-1}. (d) Electrochemical impedance spectra for symmetric pristine Al and pretreated Al cells.

The electrochemical pretreatment of the Al-graphite cells was performed at different bias potentials of 1 V, 2.5 V and 4 V for 5 min duration in 1 M $AlCl_3$ aqueous electrolyte. The application of the bias potential induces expansion of the graphite foil with maximum expansion obtained at 4 V. Galvanostatic discharge/charge experiments were now performed with these electrochemically treated Al-graphite foam cells at current density of 0.5 Ag^{-1}. These cells show varying

degree of electrochemical activities. Figure 2.1.6a shows the discharge/charge profiles of a pretreated Al-graphite foam cell (with bias of 4 V). The first discharge and charge capacities are 122 $mAhg^{-1}$ and 95 $mAhg^{-1}$ respectively. The variation of specific capacities with cycle number (Figure 2.1.6b) indicates an initial gradual decrease of specific capacities, but stability is reached after 10^{th} cycle with a stable discharge capacity of 18 $mAhg^{-1}$ at 100^{th} cycle. Again, it is also seen that the first discharge cycle shows a long discharge plateau approximately at 1.80 V. In subsequent cycles, only a kink at 1.80 V could be noticed. It is also supported by the CV profile of the cell (Figure 2.1.6c), where one pair of cathodic and anodic redox peaks approximately at 1.85 V (vs Al) is noticed. The charge capacity is relatively higher than the discharge capacity, which may be attributed to the side reaction of the electrolyte and significant gas evolution during charging/discharging could be noticed as shown in Figure 2.1.7. The discharge/charge profiles and capacity variation of the Al-graphite foam cells (with bias of 1 V and 2.5) are shown in Figure 2.1.8. These cells show lower discharge capacities (~ 10 or < 10 $mAhg^{-1}$) and the discharge plateau at 1.8 V is also found to be missing.

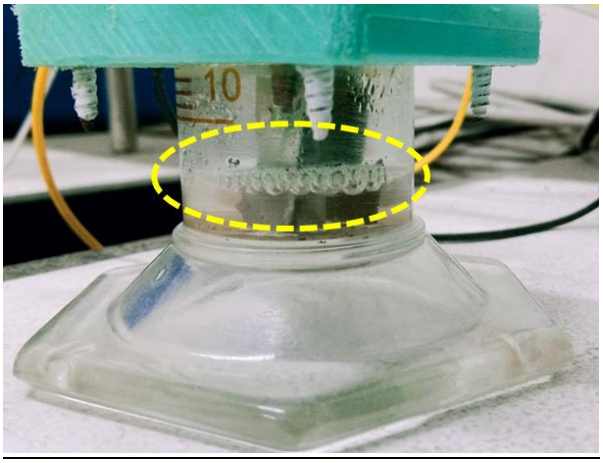

Figure 2.1.7 Digital photograph of an Al-graphite cell where gas bubble formation (marked by the dotted line) could be observed during discharge/charge experiment.

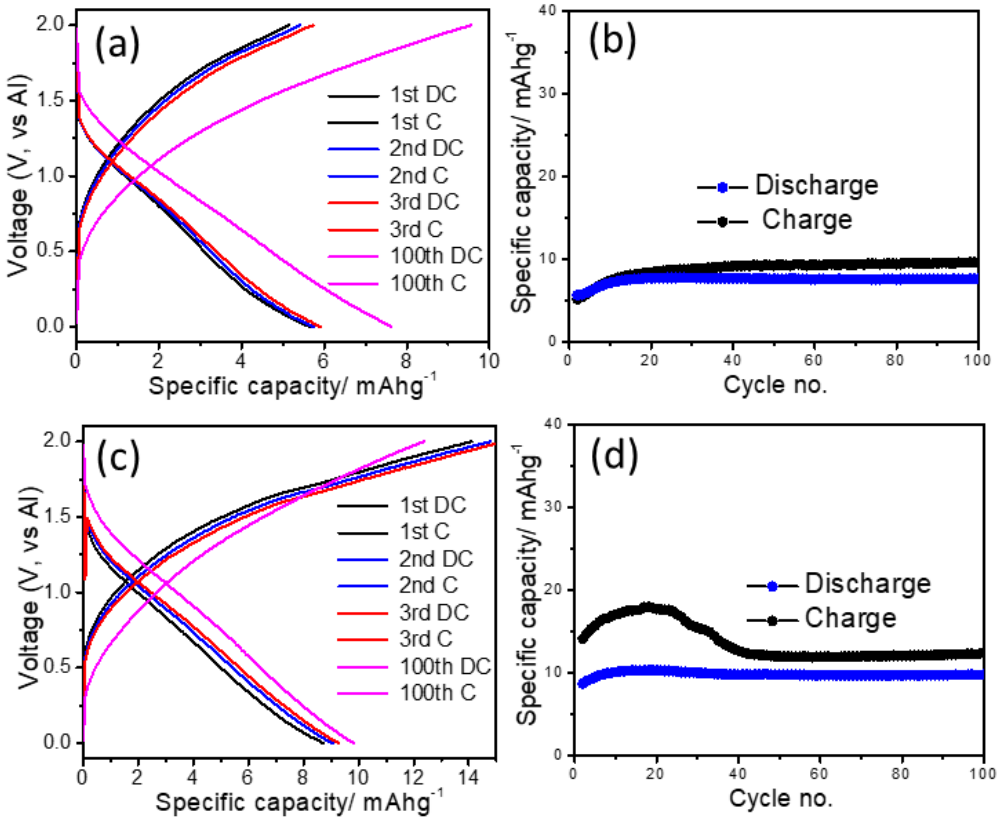

Figure 2.1.8 Galvanostatic discharge/charge curves of Al-graphite cells which are biased with a potential of (a) 1 V and (c) 2.5 V. Variation of discharge/charge capacities with cycle number with a bias potential of (b) 1 V and (d) 2.5 V. The current density is 0.5 Ag^{-1}.

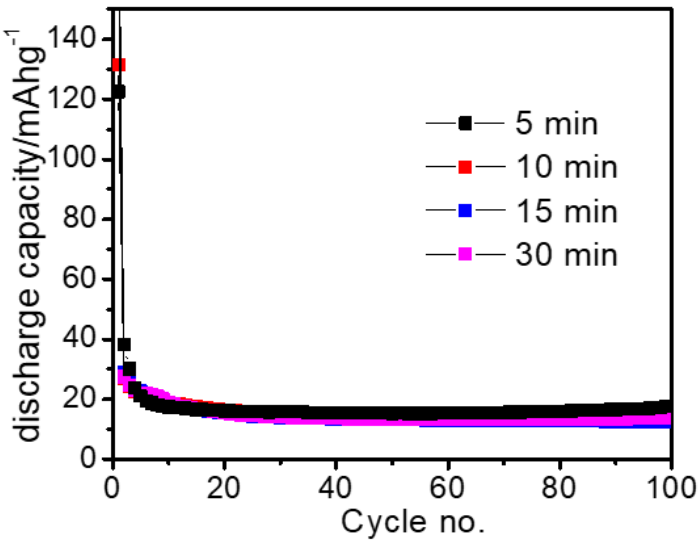

Figure 2.1.9 Variation of discharge capacities with cycle number for Al-graphite cells pretreated at different time durations but with constant bias of 4 V. The specific current density is 0.5 Ag^{-1}.

Considering the bias potential of 4 V as an optimum, Al-graphite cell was further treated for different duration e.g., 10 min, 15 min, and 30 min. As shown in Figure 2.1.9, the specific capacities are independent of the pretreatment time. Hence, further experiments with Al-graphite foam cells were restricted to time duration of 5 min only.

The obvious question at this stage is: "Why does the Al-graphite foam cell work better upon pretreatment with applied bias potential?". Is there also any effect of the pretreatment on the Al electrode apart from inducing expansion of the graphite foil? The XRD pattern of the pretreated Al electrode indicates no change of crystallinity in comparison to pristine Al (Figure 2.1.10). However, a stark contrast on surface morphology of the Al electrode before and after pretreatment could be noticed. The SEM images (Figure 2.1.11) indicate pretreated Al attains a porous surface, whereas pristine Al has smooth surface. The digital photograph also indicates bleaching of the pretreated Al electrode (Inset of Figure 2.1.11b). It is well-known that metallic Al is prone to spontaneously form a thin Al_2O_3 layer on its surface and this layer mostly prevents the electrochemical activity of Al. It is noted here that the pretreatment is performed in aqueous solution of 1 M $AlCl_3$ and chloride anion induced pitting corrosion of Al is a well-known phenomenon [32]. Therefore, it is expected that the Cl^- anions are responsible for the corrosion of the oxide layer. In order to further ascertain it, the pretreatment was performed again in 0.5 M $Al_2(SO_4)_3$ and 1 M $Al(NO_3)_3$ aqueous solutions. The pretreated Al electrodes were again examined by electron microscopy. In contrast to the previous case of pretreatment, SEM images (Figure 2.1.11c and 2.1.11d) indicate negligible change in the surface morphology of the Al electrodes pretreated in $Al_2(SO_4)_3$ and $Al(NO_3)_3$ aqueous electrolytes. Hence, the pretreatment process, performed in $AlCl_3$ aqueous solution, possibly rejuvenates the electrochemical activity of Al by considerably eroding the oxide layer by Cl^- anions. If this is true, the removal of oxide layer would consequently reduce the charge transfer resistance at electrolyte-Al electrode interface. It is well verified from EIS measurements of symmetric pristine Al and pretreated Al cells. Figure 2.1.6d (or Figure 2.1.12) shows that the charge transfer resistance is lower for the pretreated Al cell (490 Ωcm^{-2}) than pristine Al cell (773 Ωcm^{-2}).

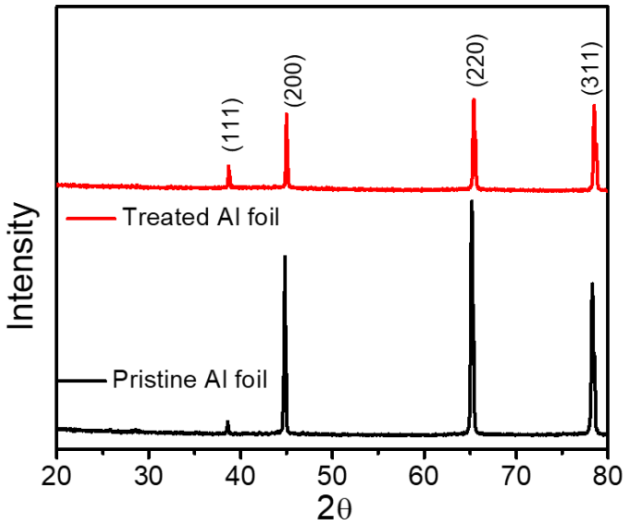

Figure 2.1.10 XRD patterns of pristine Al foil and pretreated Al foil.

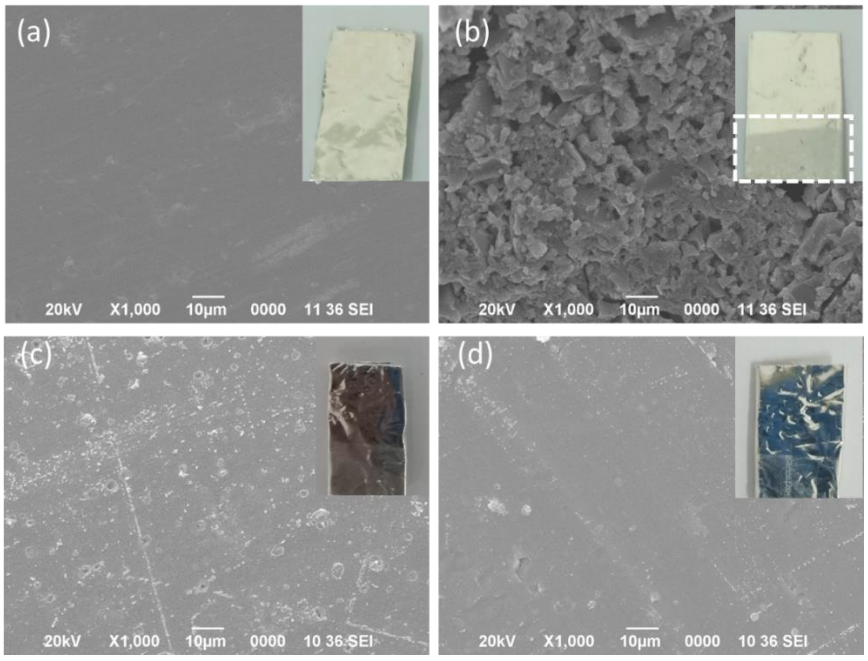

Figure 2.1.11 SEM images of (a) pristine Al foil and pretreated Al foils in (b) 1 M $AlCl_3$, (c) 0.5 M $Al_2(SO_4)_3$ and (d) 1 M $Al(NO_3)_3$ aqueous electrolytes. Insets show the digital photographs of the Al foils used in the experiments. The dotted region indicates the bleaching portion of pretreated Al foil in $AlCl_3$ electrolyte.

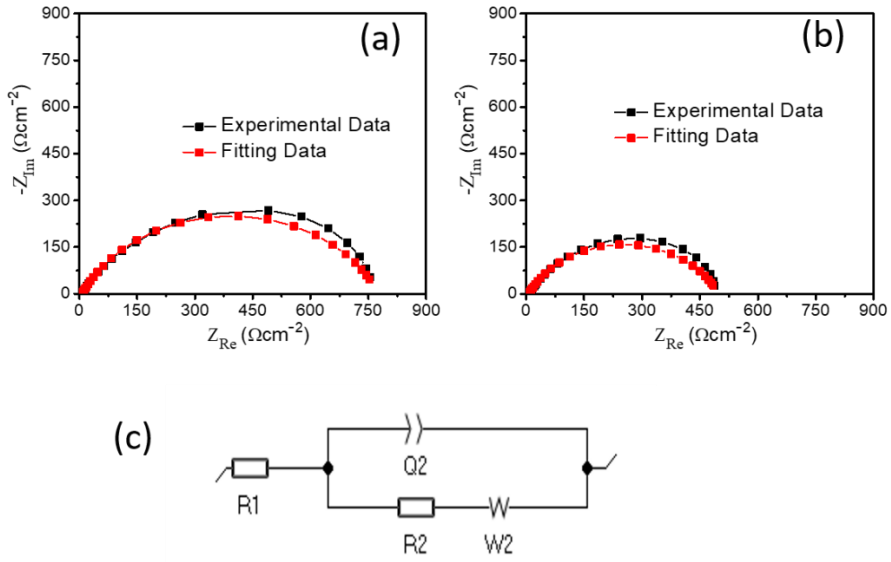

Figure 2.1.12 Electrochemical impedance spectra (EIS) for symmetric (a) pristine Al cell and (b) pretreated Al cell. (c) circuit diagram of the equivalent electrical circuit used to fit the experimental data. Here R2 corresponds to the charge transfer resistance value.

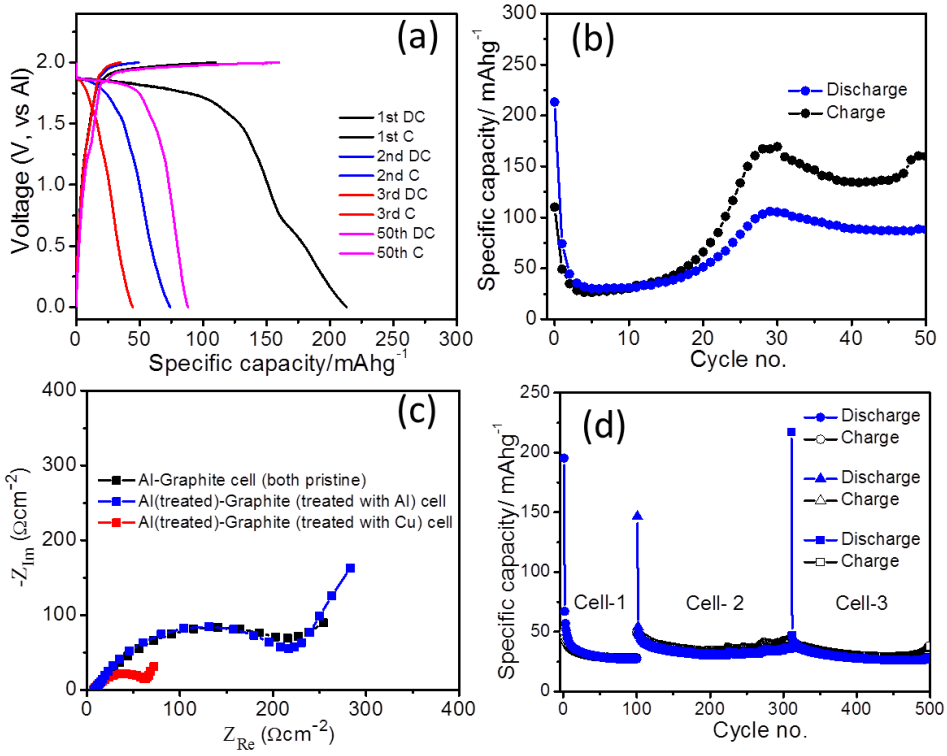

Figure 2.1.13 Galvanostatic discharge/charge curves of pretreated Al-graphite foam cell (exfoliation done with Cu), (b) Variation of discharge/charge capacities with cycle number. The current density is 0.5 Ag^{-1}. (c) Electrochemical impedance spectra for Al (pristine)-graphite (pristine) cell, Al (treated)-graphite foam (treated with Al)

cell, and Al (treated)-graphite foam (treated with Cu) cell. (d) Variation of discharge/ charge capacities with cycle number for Al-graphite foam cell by replacing Al anode after corrosion. Cell-1, Cell-2 and Cell-3 utilized same exfoliated graphite foam electrode but Al was replaced after corrosion. The current density in this case is 1 Ag^{-1}.

Exfoliation of graphite foil was also performed with Cu as counter electrode and a relatively higher expansion was observed as mentioned earlier. An Al-graphite foam cell was assembled with Al (pretreated at 4 V) and exfoliated graphite foam with Cu in 1 M $AlCl_3$ aqueous electrolyte. Figure 2.1.13a shows the discharge/charge profiles of this cell at current density of 0.5 Ag^{-1}. In this case also, a discharge plateau at 1.8 V could be observed, which is again supported by the CV profile of the cell (Figure 2.1.14) where a sharp cathodic peak could be seen at 1.82 V (vs Al). Interestingly, the discharge capacity is considerably higher than the previous cases. The discharge capacity is 88 $mAhg^{-1}$ at 50^{th} cycle (Figure 2.1.13b). These values are comparable to the initial studies of Lin et al. and Sun et al. for chloroaluminate electrolyte-based Al-ion battery with graphene and carbon paper cathodes respectively [1, 6]. Electrochemical impedance spectra were recorded for Al (pristine)-graphite (pristine) cell, Al (treated)-graphite (treated with Al) cell, and Al (treated)-graphite (treated with Cu) cell to determine the charge transfer resistance (R_{ct}). As could be seen from Figure 2.1.13c, Figure 2.1.15 and Table 2.1.1, the R_{ct} value is lowest for Al (treated)-graphite (treated with Cu) cell. It signifies the importance of exfoliation of the graphite foil in improving the storage capacity.

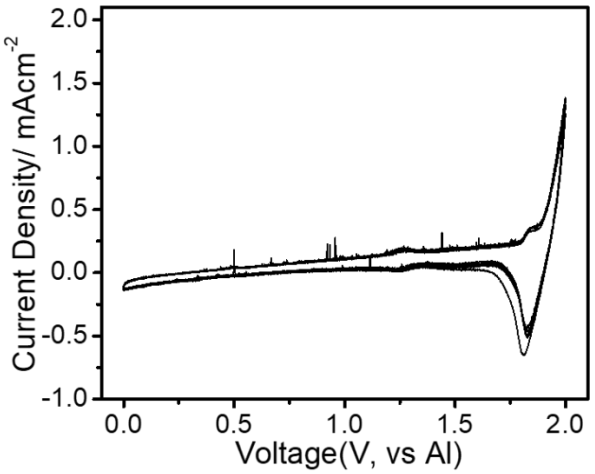

Figure 2.1.14 CV curves of Al-graphite foam cell (biased with Cu) at a scan rate of 1 mVs^{-1}.

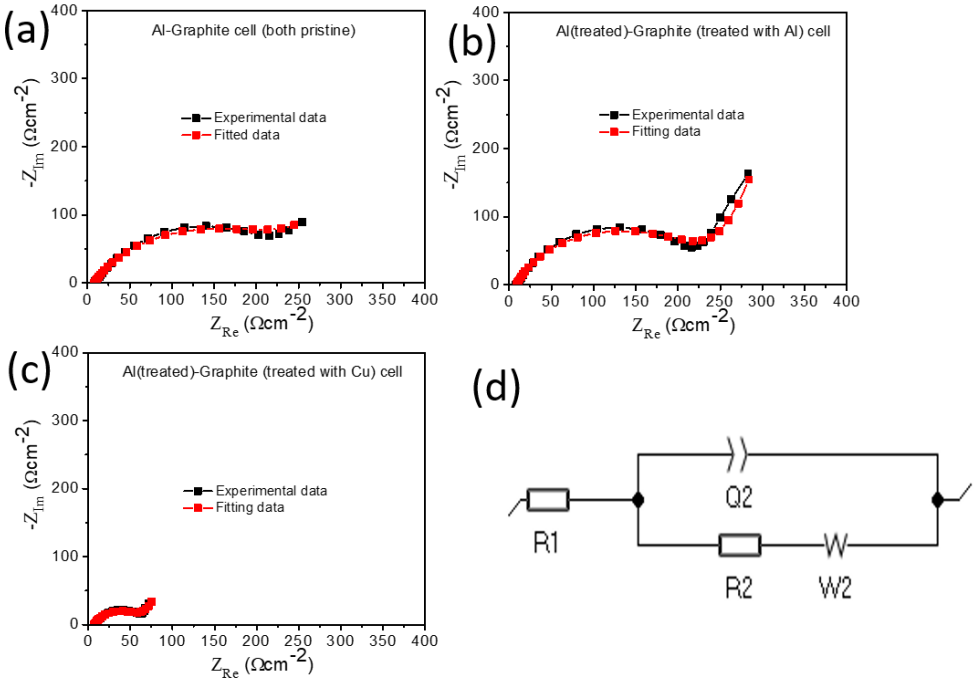

Figure 2.1.15 Electrochemical impedance spectra for (a) Al (pristine)-graphite (pristine) cell, (b) Al (treated)-graphite (treated with Al) cell and (c) Al (treated)-graphite (treated with Cu) cell. (d) circuit diagram of the equivalent electrical circuit used to fit the experimental data. Here R2 corresponds to the charge transfer resistance (R_{ct}) value.

Table 2.1.1 Charge transfer resistance (R_{ct}) values estimated from fitting the data shown in Figure 2.1.15 and using the equivalent electrical circuit shown in Figure 2.1.15d.

Sl. No.	**Cells**	**R_{ct} ($ohmcm^{-2}$)**
1.	Al(treated)-Graphite (treated with Cu)	54.32
2.	Al(treated)-Graphite (treated with Al)	222.8
3.	Al-Graphite (both pristine)	235.7

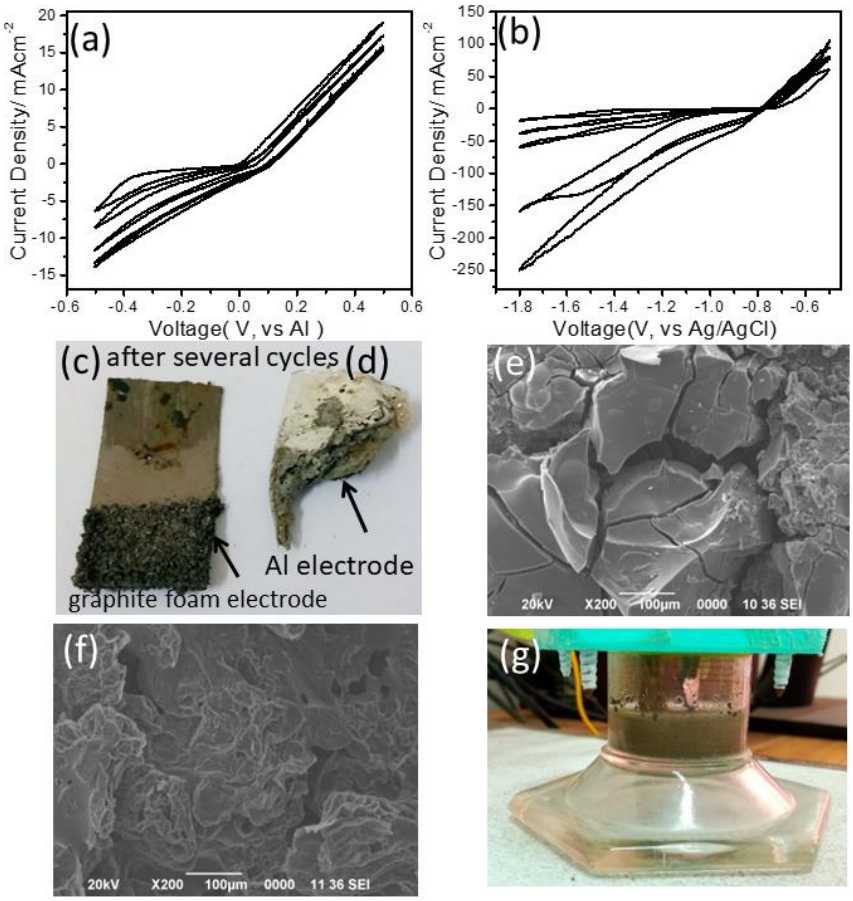

Figure 2.1.16 (a) CV curves with Al as working electrode, Pt electrode and aqueous Ag/AgCl electrode as counter and reference electrodes respectively in 3-electrode system at a scan rate of 2.5 mVs^{-1} in 1 M $AlCl_3$ aqueous electrolyte. (b) CV curves of a symmetric Al-Al cell in 1 M $AlCl_3$ aqueous electrolyte at a scan rate of 2.5 mVs^{-1}. Digital photographs of (c) exfoliated graphite foam electrode and (d) Al electrode after several cycles. SEM images of (e) Al electrode and (f) exfoliated graphite foam electrode after 50th discharge cycle, and (g) Digital photograph of used electrolyte after 50th discharge cycle

Two pertinent questions arise at this stage regarding the rechargeability of the Al-graphite cell. First, does reversible electrodeposition of Al on Al electrode occur in the used aqueous electrolyte? Second, what about the long-term cycling stability of the cell? CV experiments were performed to investigate plating and stripping of Al electrode in 1 M $AlCl_3$ aqueous electrolyte. However, CV profiles (Figure 2.1.16a, 2.1.16b) indicate no Al reduction and Al oxidation peaks, which could be otherwise prominently observed in chloroaluminate based ionic liquid electrolytes [1, 8, 13]. It does suggest that reversible electrodeposition of Al does not occur. An observation

(Figure 2.1.16d) of the Al electrode after several charge/discharge cycles (typically after 50 cycles) shows severe corrosion of Al electrode. SEM images (Figure 2.1.16e) of the Al electrode after discharge show severe multiple cracks on the surface. The electrolyte also turns greyish after few charge/discharge cycles (Figure 2.1.16g). On the other hand, the exfoliated graphite foam electrode retains its original macroscopic structure after cycling (Figure 2.1.16c) and SEM examination shows negligible change in the surface morphology (Figure 2.1.16f). Because of the severe corrosion of the Al electrode, the Al-graphite cell sustains only few cycles (typically 50-100 cycles). Hence, long-term cycling stability of Al-graphite foam cell in $AlCl_3$ aqueous electrolyte is limited by the dissolution of Al electrode. Nevertheless, this battery system is still promising and long-term sustainability could be essentially achieved by mechanically recharging the Al-graphite foam cell. Since the exfoliated graphite foam electrode suffers no physical damage after cycling, the corroded Al electrode could subsequently be replenished by a fresh piece of Al electrode. Figure 2.1.13d shows such capacity variation of a single exfoliated graphite foam electrode after replacement of corroded Al electrodes for three times. This way the sustainability of Al-graphite foam cell could be achieved beyond 500 cycles with discharge capacity of 25 $mAhg^{-1}$ at a current density of 1 Ag^{-1}.

The storage of charged species in the graphite electrode is also verified using various techniques. First, direct visual evidence of presence of Al in the exfoliated graphite foam electrode is obtained by annealing a discharged (5^{th}) state graphite electrode at 800 ^oC in air. The initially black discharged state graphite foam electrode turned completely white (or light greyish) after annealing as shown in Figure 2.1.17a. Moreover, the annealed product also retains the original macroscopic structure of the exfoliated graphite electrode. The XRD pattern (Figure 2.1.17b) of the white (or light greyish) product matches with γ-Al_2O_3 phase (JCPDS 10-0425). It thus suggests the presence of Al species in the graphite electrode, which oxidizes to form Al_2O_3 upon annealing. Again, X-ray photoelectron spectrum (Figure 2.1.17c) of the discharged (5^{th}) state graphite electrode clearly evidenced an Al 2*p* peak at 73.5 eV, which also confirms presence of Al [1, 5]. So, is it just the Al^{3+} ion which is participating in the charge/discharge processes? Ex-situ XRD measurements were performed to investigate any structural changes of the graphite electrode during cycling. As shown in Figure 2.1.17d, the discharged (5^{th}) state graphite foam electrode retains the

original graphitic structure. Contrarily, the charged (5^{th}) state graphite foam electrode shows complete disappearance of (002) graphitic peak at $2\theta = 26.33^{o}$. Instead, there is concomitant appearance of two new diffraction peaks positioned at 25.03^{o} and 27.52^{o} (Figure 2.1.17d). Similar splitting of (002) peak was also observed due to chloroaluminate anion intercalation in graphite [1, 5]. The splitting of the (002) peak during charge suggests intercalation of other charged species than Al^{3+}. It is well-known that graphite can electrochemically host large number of anions such as PF_6^-, $TFSI^-$, ClO_4^- etc. [33]. In this case, the Cl^- anion may intercalate during charging and subsequently it deintercalates during discharging. There are also certain examples of Cl^- anion intercalation in graphite [34-35]. Therefore, both Al^{3+} and Cl^- ions may participate during charge and discharge. It could be noted here that splitting of the (002) peak could not be observed during discharge may be because of the smaller ionic radius of Al^{3+} ion in comparison to Cl^- ion. Elemental mapping also suggests the possibility of involvement of both Al^{3+} and Cl^- ions. Figure 2.1.18c indicates comparatively large trace of Al in the 1^{st} discharged state graphitic foam electrode than the 1^{st} charged state electrode (Figure 2.1.18g). On the other hand, the reverse could be observed for Cl (Figure 2.1.18d). It is noted here that a trace amount of Cl is unavoidable in the 1^{st} discharged state graphitic foam since the pretreatment was performed in $AlCl_3$ solution and it is hard to wash off the adsorbed chloride on the graphitic surface. Overall, the electrochemical reactions undergoing in the aqueous Al-graphite cell could be summarized in following manner. During discharge, Al^{3+} ions are liberated from Al anode ($Al \rightarrow Al^{3+} + 3e^-$). According to Pourbaix diagram of Al and water system, it is possible for Al metal to produce Al^{3+} ions in 1 M $AlCl_3$ aqueous electrolyte since pH of 1 M $AlCl_3$ aqueous electrolyte is 3 (or < 3) [36]. The Al^{3+} ions subsequently intercalate in the graphitic cathode during discharge. On the other hand, the charging process may involve two electrochemical reactions. First, the intercalated Al^{3+} ions are released by the graphite cathode during charging. However, they do not electroplate Al on the Al anode as evidenced by the CV profiles (Figure 2.1.16a, 2.1.16b). Besides, there is no signature of deposition of additional Al compounds on the Al electrode during cycling as evidenced from ex-situ XRD measurements of the discharged/charged state Al electrode (Figure 2.1.19). Second, the Cl^- anions intercalate in graphite during charging. The severe corrosion of the Al anode may also be attributed to the attack from Cl^- anions [32, 37]. The subsequently released Cl^- anions during discharge may react with Al to form $AlCl_3$. An evidence of

it could be gathered from the comparison of the UV-visible spectra of the pristine electrolyte and harvested electrolyte after few cycles. As shown in Figure 2.1.20, the harvested electrolyte shows the characteristics of pristine electrolyte but with higher absorbance signifying presence of more concentrated electrolyte. Additional unwanted side reactions of decomposition of water molecules are also inevitable while the Al-graphite cell performs charging/discharging. This is supported by our visual observation where continuous air bubble formations were observed in both charging and discharging processes (Figure 2.1.7). Based on our experimental evidences and earlier report on halogen intercalation in graphite in aqueous media [34], the plausible electrochemical reactions occurring in the aqueous Al-graphite cell are summarized in Table 2.1.2.

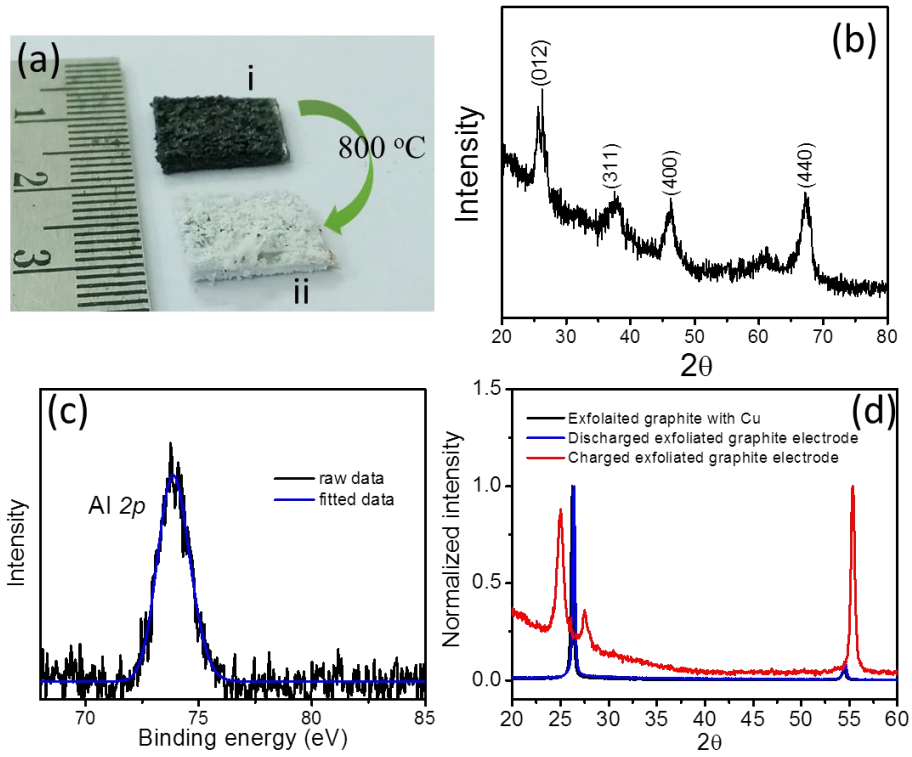

Figure 2.1.17 (a) Digital photographs of discharged state exfoliated graphite foam electrode i-before and ii-after annealing at 800 °C in air, (b) XRD pattern of the discharged state exfoliated graphite foam electrode after annealing, (c) Ex-situ XPS spectrum of Al 2*p* obtained from discharged state exfoliated graphite foam electrode, (d) Ex-situ XRD patterns of discharged and charged state exfoliated graphite foam electrodes. The XRD patterns are normalized for better visibility.

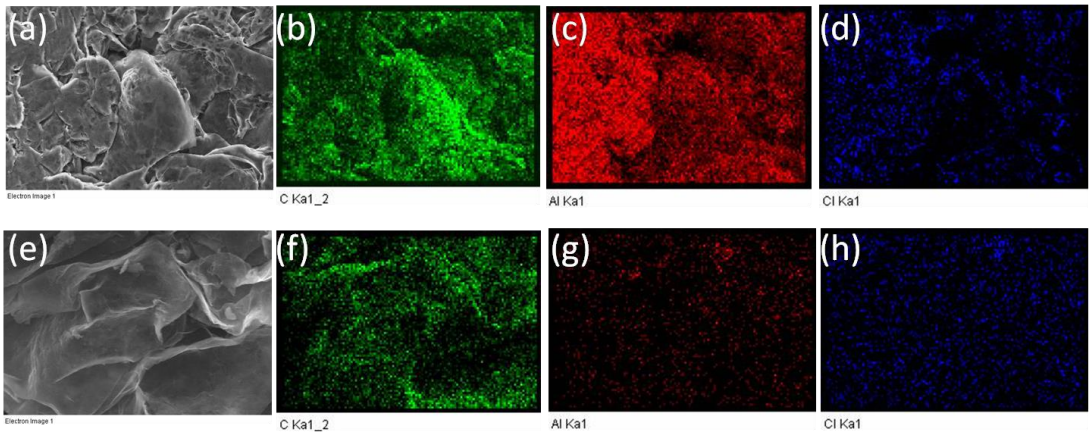

Figure 2.1.18 SEM image of scanned area for elemental mapping of 1st discharge state graphite foam electrode. Elemental mapping images of (b) C, (c) Al and (d) Cl of the 1st discharge state electrode. (e) SEM image of scanned area for elemental mapping of 1st charge state graphite foam electrode. Elemental mapping images of (f) C, (g) Al and (h) Cl of the 1st charge state electrode.

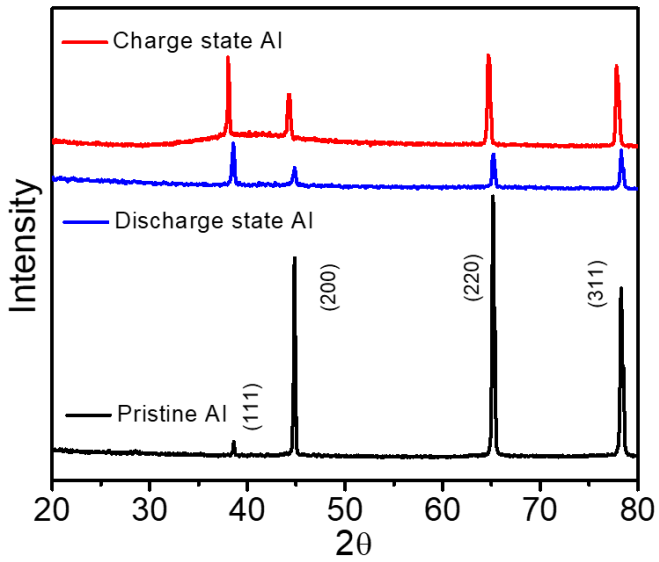

Figure 2.1.19 Ex-situ XRD patterns of Al electrode after discharge and charge.

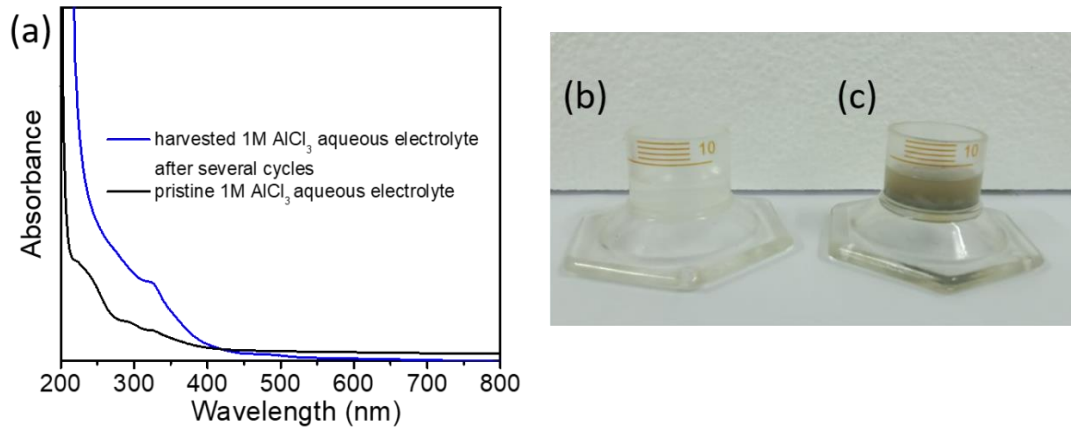

Figure 2.1.20 (a) UV-visible spectra of the pristine electrolyte and harvested electrolyte after few cycles, digital photographs of (b) pristine electrolyte and (c) harvested electrolyte after few cycles.

Table 2.1.2 Summary of possible electrochemical reactions

	Al electrode	Graphite electrode
Discharge	$Al \rightarrow Al^{3+} + 3e^-$	$C_n + Al^{3+} + 3e^- \rightarrow C_n[Al]$, n is the molar ratio of carbon atoms to intercalated Al^{3+} ions in the graphite electrode
Charge	Al does not electroplate	$C_n[Al] \rightarrow C_n + Al^{3+} + 3e^-$ and $C_m + Cl^- - e^- \rightarrow C_m[Cl]$, m is the molar ratio of carbon atoms to intercalated Cl^- ions in the graphite electrode

2.1.4 Conclusion

In conclusion, a simple and facile concept of rechargeable aqueous Al-metal battery with electrochemically pretreated Al and exfoliated graphite foam electrodes is illustrated. The long-term stability of the aqueous Al-graphite cell is found to be limited by the dissolution of Al anode, but we show greater sustainability of the system by mechanical rejuvenation of the cell. The specific capacities are relatively low (~ 88 $mAhg^{-1}$ at 0.5 Ag^{-1}/25 $mAhg^{-1}$ at 1 Ag^{-1}) compared to state-of-art Li-ion battery electrodes, but such an investigation as discussed here provide an important basis for future studies in aqueous Al-battery. The presented aqueous Al-metal battery takes the advantage of raw materials which are locally available in high abundance, low-priced, and ecofriendly. Besides, the ease in handling the materials and

assembling the battery system opens exciting opportunities for safe, sustainable, and affordable energy storage device.

2.1.5 References

[1] Lin, M. C., Gong, M., Lu, B., Wu, Y., Wang, D. Y., Guan, M., Angell, M., Chen, C., Yang, J., Hwang, B. J., and Dai, H. An ultrafast rechargeable aluminum-ion battery. *Nat.*, 520(7547):324, 2015.

[2] Yu, X., Wan g, B., Gong, D., Xu, Z., and Lu, B. Graphene nanoribbons on highly porous 3D graphene for high-capacity and ultrastable Al-ion batteries. *Adv. Energy Mater.*, 29: 1604118, 2017.

[3] Chen, H., Xu, H., Wang, S., Huang, T., Xi, J., Cai, S., Guo, F., Xu, Z., Gao, W. and Gao, C. Ultrafast all-climate aluminum-graphene battery with quarter-million cycle life. *Sci. Adv.*, 3(12):7233, 2017.

[4] Wu, Y., Gong, M., Lin, M. C., Yuan, C., Angell, M., Huang, L., Wang, D. Y., Zhang, X., Yang, J., Hwang, B. J., and Dai, H. 3D Graphitic foams derived from chloroaluminate anion intercalation for ultrafast aluminum-ion battery. *Adv. Mater.* 28: 9218-9222, 2016.

[5] Elia, G. A., Hasa, I., Greco, G., Diemant, T., Marquardt, K., Hoeppner, K., Behm, R. J., Hoell, A., Passerini, S., and Hahn, R. Insights into the reversibility of aluminum graphite batteries. *J. Mater. Chem. A*, 5(20):9682-9690, 2017.

[6] Sun, H., Wang, W., Yu, Z., Yuan, Y., Wang, S., Jiao, S. A new aluminium-ion battery with high voltage, high safety and low cost. *Chem. Commun*. 2015, 51, 11892– 11895,

[7] Yu, Z., Tu, J., Wang, C., and Jiao, S. A Rechargeable Al/graphite battery based on $AlCl_3$/1-butyl-3-methylimidazolium chloride ionic liquid electrolyte. *Chem. Select*, 4:3018-3024, 2019.

[8] Angella, M., Pana, C. –J., Ronga, Y., Yuana, C., Linc, M. –C., Hwang, B. –J., and Dai, H. High coulombic efficiency aluminum-ion battery using an $AlCl_3$-urea ionic liquid analog electrolyte. *PNAS*, 114, 834–839, 2017.

[9] Wang, W., Jiang, B., Xiong, W., Sun, H., Lin, Z., Hu, L., Tu, J., Hou, J., Zhu, H., and Jiao, S. A new cathode material for super-valent battery based on aluminum ion intercalation and deintercalation. *Sci. Reports*, 3:3383, 2013.

[10] Wang, S., Yu, Z., Tu, J., Wang, J., Tian, D., Liu, Y., and Jiao, S. A novel aluminum-ion battery: Al/$AlCl_3$-[EMIm] Cl/Ni_3S_2@ graphene. *Adv. Energy Mater.*, 6(13):1600137, 2016.

[11] Jayaprakash, N., Das, S. K., and Archer, L. A. The rechargeable aluminum-ion battery. *Chem. Commun.*, 47:12610-12612, 2011.

[12] Das, S. K., Mahapatra, S., and Lahan, H. Aluminium-ion batteries: developments and challenges. *J. Mater. Chem. A*, 5:6347– 6367, 2017.

[13] Jiang, T., Brym, M. C., Dube, G., Lasia, A., and Brisard, G. M. Electrodeposition of aluminium from ionic liquids: Part I—electrodeposition and surface morphology of aluminium from aluminium chloride ($AlCl_3$)–1-ethyl-3-methylimidazolium chloride ([EMIm] Cl) ionic liquids. *Surf. Coat. Technol.*, 201, 1-9, 2006.

[14] Wilkes, J. S., Levisky, J. A., Wilson, R. A., Hussey, C. L. Dialkylimidazolium chloroaluminate melts: a new class of room-temperature ionic liquids for electrochemistry, spectroscopy and synthesis. *Inorg. Chem.* 1982, 21:1263– 1264

[15] Bin, D., Wang, F., Tamirat, A. G., Suo, L., Wang, Y., Wang, C., Xia, Y. Progress in Aqueous Rechargeable Sodium-Ion Batteries. *Adv. Energy Mater*. 8:1703008, 2018

[16] Liu, J., Xu, C., Chen, Z., Ni, S., and Shen, Z. X. Progress in aqueous rechargeable batteries. *Green Energy & Environ.*, 3:20-41, 2018.

[17] ManalastasJr, W., Kumar, S., Verma, V., Zhang, L., Yuan, D., and Srinivasan, M. Water in rechargeable multivalent-ion batteries: An electrochemical pandora's box. *ChemSusChem.*, 12:379–396, 2019.

[18] Liu, S., Pan, G. L., Li, G. R., and Gao, X. P. Copper hexacyanoferrate nanoparticles as cathode material for aqueous Al-ion batteries. *J. Mater. Chem. A* 3:959-962, 2015.

[19] Ru, Y., Zheng, S., Xue, H., and Pang, H. Potassium cobalt hexacyanoferrate nanocubic assemblies for high-performance aqueous aluminum ion batteries. *Chem. Engineer. J.*, 382:122853, 2019.

[20] Holland, A., Mckerracher, R. D., Cruden, A., and Wills, R. G. A. An aluminum battery operating with an aqueous electrolyte. *J. Appl. Electrochem.*, 48(3):243-250, 2018.

[21] Kumar, S., Satish, R., Verma, V., Ren, H., Kidkhunthod, P., Manalastas, Jr. W., and Srinivasan, M. Investigating $FeVO_4$ as a cathode material for aqueous aluminum-ion battery. *J. Power Sources*, 426: 151– 161, 2019.

[22] Pang, Q., Yang, S., Yu, X., He, W., Zhang, S., Tian, Y., Xing, M., Fu, Y., and Luo, X. Realizing reversible storage of trivalent aluminum ions using $VOPO_4 \cdot 2H_2O$ nanosheets as cathode material in aqueous aluminum metal batteries. *J. Alloys and Comp.*, 885:161008, 2021.

[23] Lahan, H., and Das, S. K. Al^{3+} ion intercalation in MoO_3 for aqueous aluminium-ion battery. *J. Power Sources*, 413:134-138, 2019.

[24] Nacimiento, F., Cabello, M., Alcántara, R., Lavela, P., and Tirado, J. L. NASICON-type $Na_3V_2(PO_4)_3$ as a new positive electrode material for rechargeable aluminum battery. *Electrochim. Acta*, 260:798-804, 2018.

[25] Soundharrajan, V., Nithiananth, S., Lee, Kim, J.H., Hwang, J.-Y., and Kim, J. LiV_3O_8 as an intercalation-type cathode for aqueous aluminum-ion batteries. *J. Mater. Chem. A*, 2022: 18162-18169, 10.

[26] Zhao, Q., Zachman, M. J., Sadat, W. I. Al., Zheng, J., Kourkoutis, L. F., and Archer, L. Solid electrolyte interphases for high-energy aqueous aluminum electrochemical cells. *Sci. Adv.*, 4:8131, 2018.

[27] Wu, C., Gu, S., Zhang, Q., Bai, Y., Li, M., Yuan, Y., Wang, H., Liu, X., Yuan, Y., Zhu, N., Wu, F., Li, H., Gu, L., Lu, J., Electrochemically activated spinel manganese oxide for rechargeable aqueous aluminum battery. *Nat. Commun.*, 10:73, 2019.

[28] Li, Q., and Bjerrum, N. J. Aluminum as anode for energy storage and conversion: a review. *J. Power Sources*, 110: 1–10, 2002.

[29] Eftekhari, A., and Corrochanoc, P. Electrochemical energy storage by aluminum as a lightweight and cheap anode/charge carrier. *Sust. Energy Fuels*, 1: 1246-1264, 2017.

[30] Bard, A. J., Faulkner, L. R., Leddy, J., and Zoski, C. G. Electrochemical Methods: Fundamentals and Applications. John Wiley & Sons, Inc., *New York*, 1980.

[31] Rudolph, W. W., Mason, R., and Pye, C. C. Aluminium(III) hydration in aqueous solution. A raman spectroscopic investigation and an ab initio molecular orbital study of aluminium (III) water clusters. *Phys. Chem. Chem. Phys.* 2: 5030-5040, 2000.

[32] Natishan, P. M., and O'Grady, W. E. Chloride ion interactions with oxide-covered aluminum leading to pitting corrosion: a review. *J. Electrochem. Soc.*, 161: 421-432, 2014.

[33] Li, Y., Lu, Y., Adelhelm, P., Titirici, M. M., and Hu, Y. S. Intercalation chemistry of graphite: alkali metal ions and beyond. *Chem. Soc. Rev.*, 48:4655-4687, 2019.

[34] Yang, C., Chen, J., Ji, X., Pollard, T.P., Lu, X., Sun, C. J., Hou, S., Liu, Q., Liu, C., Qing, T., Wang, Y., Wang, Y., Borodin, O., Ren, Y., Xu, K., and Wang, C. Aqueous Li-ion battery enabled by halogen conversion-intercalation chemistry in graphite. *Nat.*, 569:245-250, 2019.

[35] Furdin, G., Lelaurain, M., McRae, E., Marcehe, J. F., and Herold, A. Insertion du chloredans le graphite. *Carb.,* 17: 329-333, 1979.

[36] Deltombe, E., and Pourbaix, M. The electrochemical behavior of aluminum—potential pH diagram of the system AI-H_2O at 25 ^oC. *Corros.*, 14:16-20, 1958.

[37] Atanasoska, Lj. D.; Drazic, D. M.; Despic, A. R.; and Zalar, A. Chloride ion penetration into oxide films on aluminum: Auger and XPS studies. *J. Electroanal. Chem.*, 182:179-186, 1985.

Chapter 2 (Part II)

A simple strategy to improve the electrochemical performance of rechargeable aqueous aluminum-metal battery

Nandi, S and Das, S. K. *Material Letters,* 301:130263, 2021.

A simple strategy to improve the electrochemical performance of rechargeable aqueous aluminum-metal battery

2.2.1 Introduction

In the previous chapter, a simple and novel concept of rechargeable aqueous aluminum (Al)-metal battery with graphitic foam as cathode was demonstrated and it was observed that only electrochemically pretreated graphite showed considerable Al^{3+} ion storage capability than pristine graphite. However, the specific capacities obtained in aqueous Al-metal/ion battery were certainly low compared to the state-of-the-art lithium-ion batteries (LIBs). Therefore, in an effort to improve the electrochemical performance of the battery in aqueous electrolyte, this chapter discusses a facile strategy to boost the storage capacity of Al^{3+} ion by simple modification of the graphite electrode via electrochemical exfoliation followed by thermal treatment. When the thermally exfoliated graphite was used as a cathode in an Al-cell, it shows superior performance in comparison to exfoliated graphite and pristine graphite. The influence of 'water-in-salt' electrolyte in the aqueous Al-metal battery was also investigated.

2.2.2 Experimental Section

2.2.2.1 Materials

The electrochemical exfoliation process of graphite was reported in the previous chapter. Briefly to describe, a dc potential (3 V) was applied between a Cu and pristine graphite electrode (dimension = 1 cm × 1.5 cm) in 1 M $AlCl_3$ aqueous electrolyte for 5 min. This resulted in expansion of the graphite electrode, which is termed as exfoliated graphite (EG). This EG electrode was further treated at 800 °C for less than 1 min in ambient atmosphere which resulted in further expansion of the EG. It is termed as thermally exfoliated graphite (TEG). Both EG and TEG were directly used as cathode for electrochemical investigations.

2.2.2.2 Characterization

The crystallographic phase identification was performed by using powder X-ray diffraction (BRUKER AXS D8 FOCUS; Cu-K_α radiation, λ = 1.5406 Å). The morphology was observed by field emission scanning electron microscopy (FESEM,

FESEM, JEOL JSM 7200F) and transmission electron microscopy (TEM, JOEL JEM 2100). Quantification of specific surface areas (BET) of pristine graphite and exfoliated graphite was done from N_2 adsorption-desorption isotherms (Quantachrome, NOVA 1000E).

2.2.2.3 Electrochemical analysis

Cyclic voltammetry (CV) and galvanostatic discharge/charge experiments were performed in a two-electrode glass cell in the voltage range of 0.05-2 V. The utilized electrolyte was 1 M $AlCl_3$ aqueous electrolyte unless otherwise explicitly stated. 'Water-in-salt' (WiS) electrolyte was prepared by mixing 2.41 g of $AlCl_3.6H_2O$ in 10 ml of deionized water. Electrochemical impedance spectra (EIS) were recorded in frequency range of 1 mHz-200 kHz at 10 mV signal amplitude. All the electrochemical experiments were conducted at 25 ^oC and ambient atmosphere.

2.2.3 Results and Discussion:

As described in the previous chapter, the electrochemical exfoliation process resulted in the expansion of the pristine graphite. The thermal treatment resulted in further expansion of the electrochemically exfoliated graphite. The thicknesses of the TEG and EG are respectively 440% and 248% larger compared to pristine graphite shown in Figure 2.2.1. Both of them resemble a foam type macrostructure.

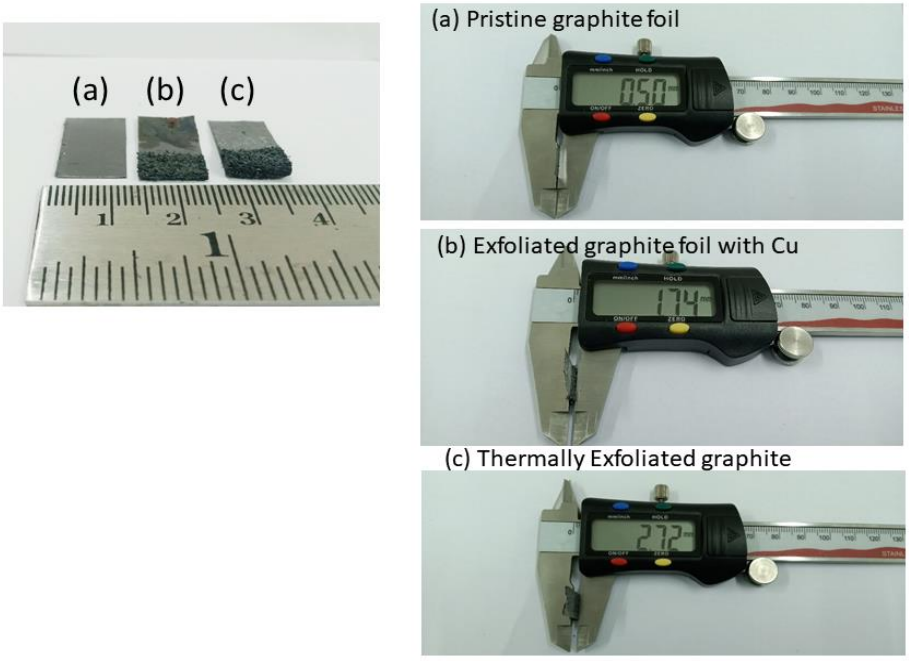

Figure 2.2.1 Digital photographs and thickness measurement of (a) pristine graphite, (b) exfoliated graphite and (c) thermally exfoliated graphite films.

SEM investigation shows presence of nanosized flake or crumbled sheet on the surface of electrochemically EG and TEG (Figure 2.2.2a, b). TEM image shows one such crumbled sheet (Figure 2.2.2c). N_2 adsorption/desorption isotherms (Figure 2.2.2d) indicate that the BET surface area of TEG (~ 55.54 m^2g^{-1}) is higher than the surface area of EG (~ 39 m^2g^{-1}) and pristine graphite (~ 29 m^2g^{-1}) which indicates the existence of a large number of mesopores and very little micropores in graphite-based adsorbents due to more porous nature of TEG. However, XRD patterns (Figure 2.2.3) indicate the same graphitic structure for all the graphite films. The exfoliation due to thermal treatment is because of the evaporation induced pressure by the decomposed oxygenated functionalities of graphitic layers, which weakens the van der Waals force between adjoining graphitic sheets [1].

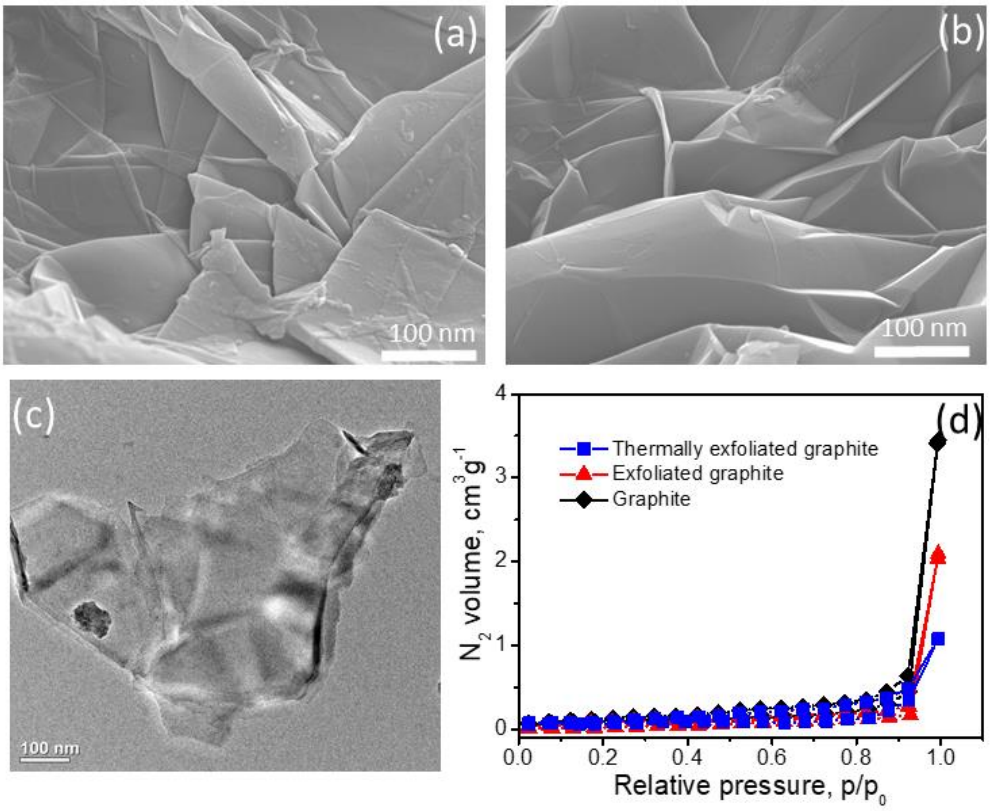

Figure 2.2.2 FESEM images of (a) EG and (b) TEG. (c) TEM image of nanoflakes. (d) BET isotherms of all graphitic films.

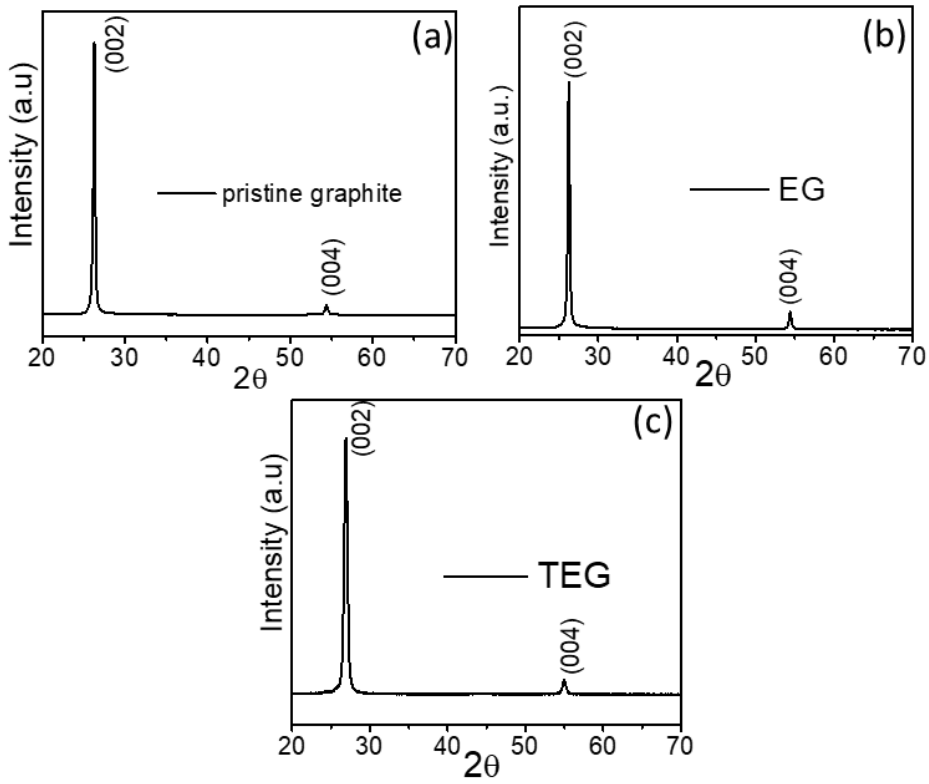

Figure 2.2.3 XRD patterns of (a) pristine graphite, (b) exfoliated graphite (EG) and, (c) thermally exfoliated graphite (TEG).

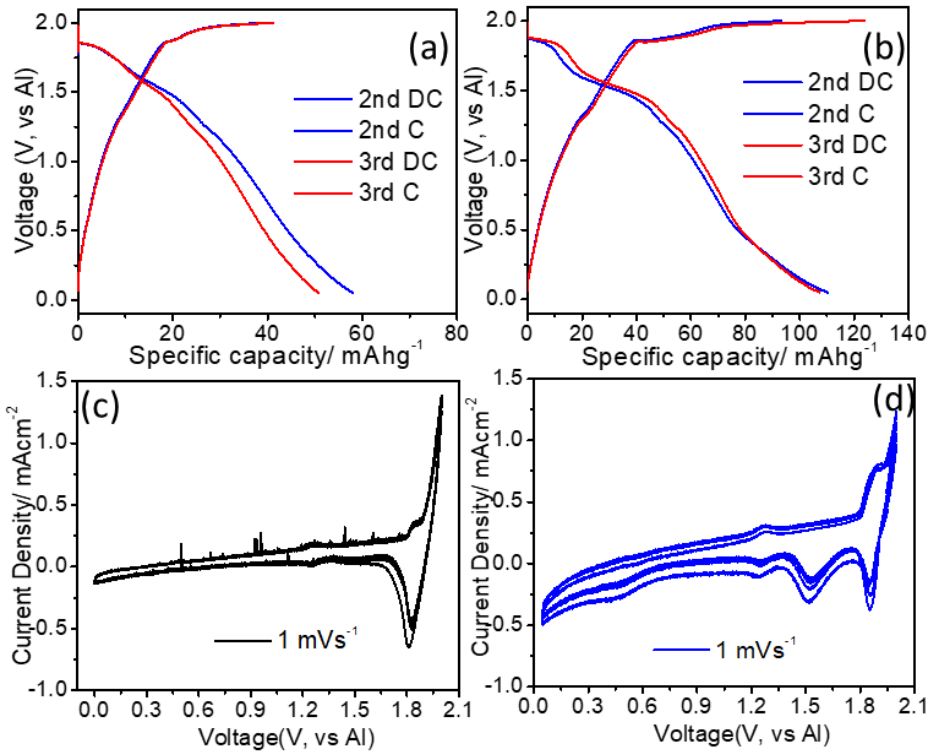

Figure 2.2.4 Galvanostatic discharge/charge profiles of (a) Al-EG and (b) Al-TEG at a current density of 0.5 Ag^{-1} current. CV profiles of (c) Al-EG (from previous chapter) and (d) Al-TEG at a scan rate of 1 mVs^{-1} scan rate in 1 M $AlCl_3$ aqueous electrolyte.

Figure 2.2.4 (a, b) shows the discharge/charge profiles of Al-EG and Al-TEG cells in 1 M $AlCl_3$ aqueous electrolyte. The discharge capacity for the EG is estimated to be 50-60 $mAhg^{-1}$ for the first few cycles. Contrarily, significant improvement in the discharge capacity could be seen for TEG, where discharge capacity values are 100-120 $mAhg^{-1}$. Additionally, noticeable differences in the features of the discharge and charge curves could also be observed. Two short and long discharge potential plateaus circa at 1.85 V and 1.55 V respectively could be prominently noticed for TEG, which are not clearly visible for EG. This type of potential plateaus was also seen for graphene-based electrodes in chloroaluminate electrolytes [2-5]. CV profiles further corroborate the galvanostatic features. For TEG, two prominent cathodic peaks were seen at 1.53 V and 1.85 V along with a minor intensity peak at 1.25 V (Figure. 2.2.4d), whereas only one peak at 1.85 V was seen for EG (Figure 2.2.4c). In both cases, however, only one anodic peak at 1.88 V could be noticed. This signifies that Al^{3+} ion storage mechanism is an intricate process which depends on the processing condition of the graphite electrodes. Similar behavior was also reported by other groups for chloroaluminate electrolytes [2-5]. A performance comparison of the TEG electrode is given in Table 2.2.3. The improved performance for TEG is may be due to nanostructuring and high surface area, which facilitate the Al^{3+} ion diffusion. The variation of discharge capacity with cycle number at current rate of 2 Ag^{-1} (Figure 2.2.5c) and 5 Ag^{-1} (Figure 2.2.5d) clearly shows the superior performance of TEG than EG. This is again verified by EIS study (Fig. 2.2.5a). It is seen that the charge transfer resistance for Al-TEG cell is lower than the Al-EG cell.

Table 2.2.3 The electrochemical performances of other cathode materials

Cathode materials	Discharge capacity ($mAhg^{-1}$)[a] /Current density (mAg^{-1})	Discharge potential (V)	Type of electrolyte	Reference
Thermally exfoliated graphite	110/500	1.8	Aqueous electrolyte	this work
Graphene foam	60/4000	~1.8	Chloroaluminate electrolyte	4
Graphene film	110/1000	~2	Chloroaluminate electrolyte	5
Carbon paper	50/150	~1.8	Chloroaluminate electrolyte	6
V_2O_5	305/125	~0.5	Chloroaluminate electrolyte	7
MO_6S_8	148/12	~0.55	Chloroaluminate electrolyte	8
NiS	104/200	~1	Chloroaluminate electrolyte	9
V_2CT_x	100/100	~1	Chloroaluminate electrolyte	10
MnO_2	380/100	~1.3	Aqueous electrolyte	11
MnO_2	467/30	~1.1	Aqueous electrolyte	12

(a) The highest discharge capacity is mentioned

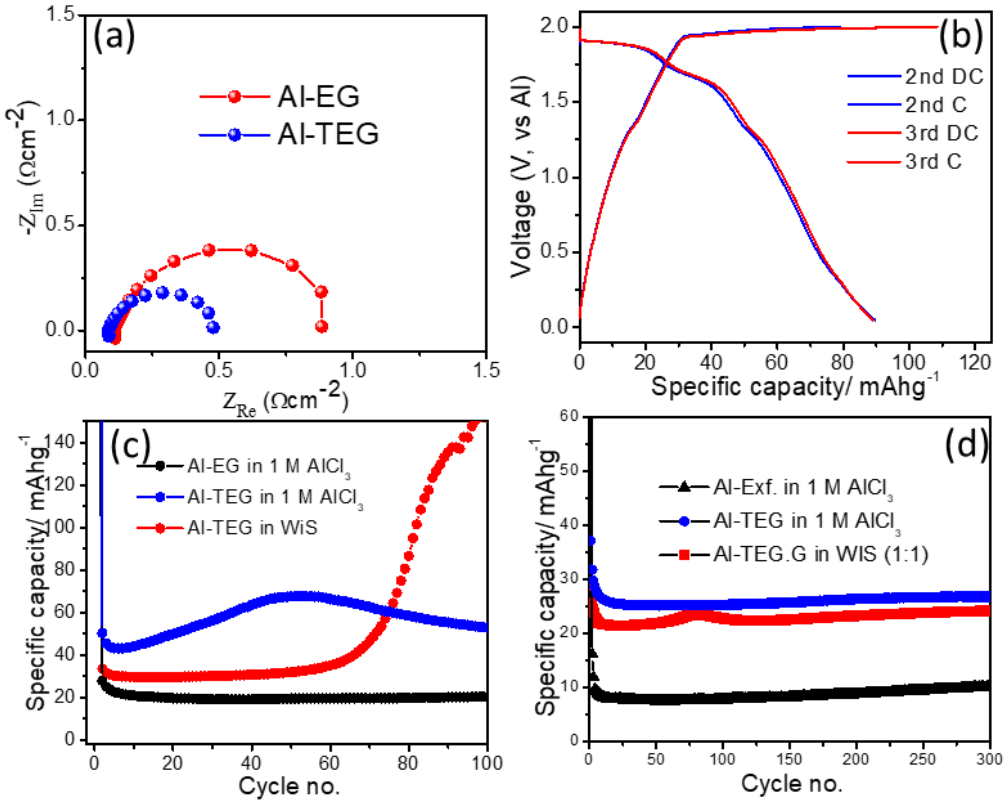

Figure 2.2.5 (a) EIS spectra for Al-EG and Al-TEG cells. (b) galvanostatic charge/discharge profile of Al-TEG in WiS electrolyte at a current density of 0.5 Ag^{-1} current. Variation of discharge capacities with cycle number for Al-EG and Al-TEG in 1 M $AlCl_3$ and WiS aqueous electrolytes at a current density of (c) 2 Ag^{-1}, and (d) 5 Ag^{-1}.

The electrochemical investigation was also performed with 'water-in-salt' (WiS) electrolyte, which is widely used recently to improve the electrochemical stability window of aqueous electrolytes [13]. Therefore, the electrochemical performance of Al-TEG cell is also investigated in WiS electrolyte (1:1). It is seen that the performance is better than EG in 1 M $AlCl_3$ aqueous electrolyte, but inferior to TEG in 1 M $AlCl_3$ aqueous electrolyte (Figure 2.2.5b). The discharge capacity is approximately 90 $mAhg^{-1}$. The discharge potential plateaus are at 1.89 V and 1.67 V, which are 0.04 V and 0.14 V higher than TEG in 1 M $AlCl_3$ aqueous electrolyte. Again, the plateau at 1.89 V is longer than 1.67 V. This again reflects the complex Al^{3+} ion insertion process. It is seen that the discharge capacity in WiS electrolyte (Fig. 2.2.5c) increases dramatically after cycling the Al-TEG cell for few cycles (> 60 cycles).

It reaches a discharge capacity of 150 $mAhg^{-1}$ at the 100^{th} cycle. However, the cell could not be cycled thereafter due to complete corrosion of the Al anode (Figure 2.2.6a). It is noted here that corrosion also occurs in 1 M $AlCl_3$ aqueous electrolyte but at a slower corrosion rate compared to WiS electrolyte. Higher concentration of WiS electrolyte (> 1:1) was not used due to spontaneous corrosion of Al. The self-discharge properties of the Al-cells were also investigated. The open circuit potentials of the cells were measured after charging to 2 V. It was found that potential drops to 0.55 V after 5 h (Figure 2.2.6b). The potential drop is serious in WiS and there is complete corrosion of Al anode after 6 h. One reason for the observed high self-discharge is due to the spontaneous corrosion of the Al metal in the highly acidic $AlCl_3$ electrolyte. Moreover, CV profiles at different scan rates are shown in Figure 2.2.6c and the linear dependence between peak current response and square of scan rates (Figure 2.2.6d) indicates a diffusion-controlled Al^{3+} ion intercalation process [14].

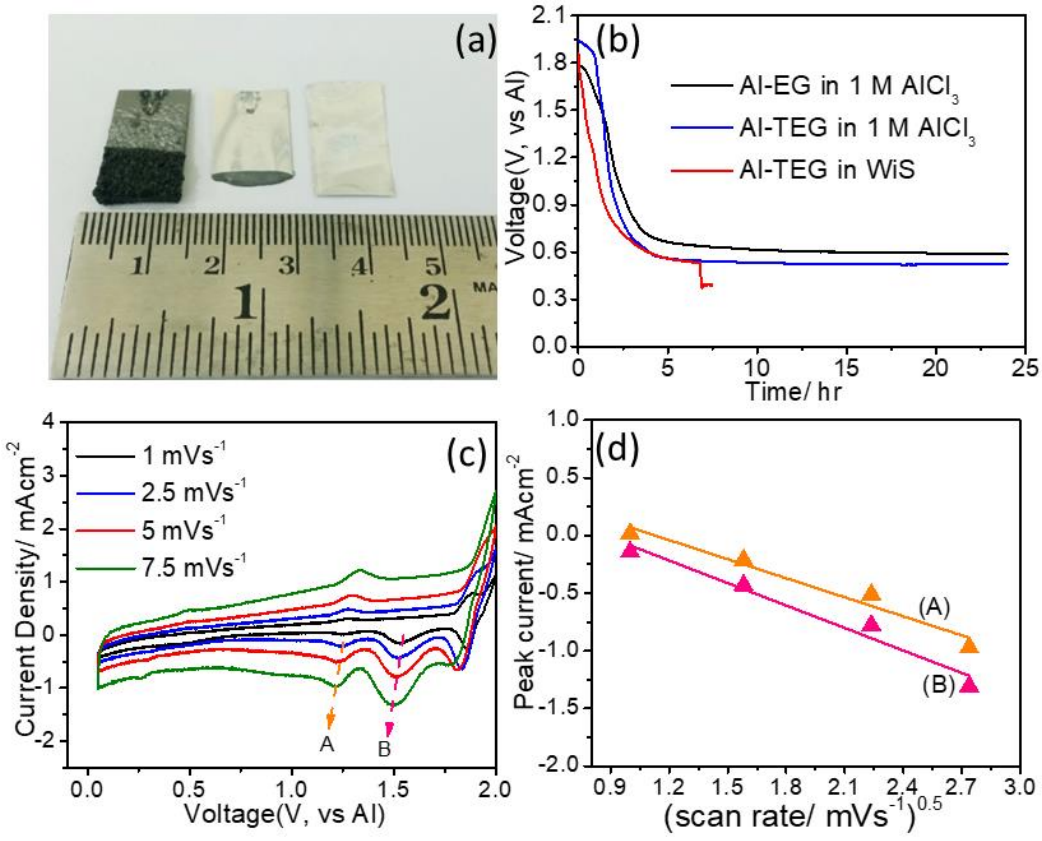

Figure 2.2.6 (a) Digital photographs of aluminum-graphite battery after several cycles in water-in-salt electrolyte, showing serious corrosion in the Al anode. (b) Self-discharge profiles of Al-graphite cells. (c) CV profiles of Al-TEG in 1 M $AlCl_3$ aqueous electrolyte at different scan rates and (d) variation of redox peak current

versus scan rate according to equation $I=k\gamma^{0.5}$ (k is a constant). The peaks (A and B) marked by the arrows are considered here.

2.2.4 Conclusion

In summary, this chapter discusses a novel electrochemical and thermally treatment method to exfoliate graphite electrode in 1 M $AlCl_3$ aqueous electrolyte which possesses high surface area. When utilized the thermally exfoliated graphite as a cathode in Al-cell, it shows superior performance in comparison to exfoliated graphite and pristine graphite. The role of WiS was also investigated which shows that severe corrosion of Al anode is a major concern. The charge/discharge profiles are also found to be different for electrochemically and thermally exfoliated graphite.

2.2.5 References

[1] Schniepp, H.C., Li, Je.-L., McAllister, M.J., Sai, H., Herrera-Alonso, M., Adamson, D.H., Prud'homme, R. K., Car, R., Saville, D.A. and Aksay, I. A. Functionalized single graphene sheets derived from splitting graphite oxide. *J. Phys. Chem. B*, 110: 8535–8539, 2006.

[2] Elia, G. A., Hasa, I., Greco, G., Diemant, T., Marquardt, K., Hoeppner, K., Behm, R. J., Hoell, A., Passerini, S., and Hahn, R. Insights into the reversibility of aluminum graphite batteries. *J. Mater. Chem. A.*, 5(20):9682-9690, 2017.

[3] Childress, A.S., Parajuli, P., Zhu, J., Podila, R., and Rao, A. M. A Raman spectroscopic study of graphene cathodes in high-performance aluminum ion batteries. *Nano. Energy*, 39:69-76, 2017.

[4] Lin, M. C., Gong, M., Lu, B., Wu, Y., Wang, D. Y., Guan, M., Angell, M., Chen, C., Yang, J., Hwang, B. J., and Dai, H. An ultrafast rechargeable aluminum-ion battery. *Nat.*, 520 (7547):324, 2015.

[5] Chen, H., Xu, H., Wang, S., Huang, T., Xi, J., Cai, S., Guo, F., Xu, Z., Gao, W., and Gao, C. Ultrafast all-climate aluminum-graphene battery with quarter-million cycle life. *Sci. Adv.*, 3(12):7233, 2017.

[6] Sun, H., Wang, W., Yu, Z., Yuan, Y., Wang, S., and Jiao, S. A new aluminium-ion battery with high voltage, high safety and low cost. *Chem. Commun.* 51:11892–11895, 2015.

[7] Jayaprakash, N., Das, S. K., and Archer, L. A. The rechargeable aluminum-ion battery. *Chem. Commun.*, 47:12610-12612, 2011.

[8] Geng, L., Lv, G., Xing, X., and Guo. J. Reversible electrochemical intercalation of aluminum in Mo_6S_8. *Chem. Mater.*, 27:4926-4929, 2015.

[9] Yu, Z., Kang, Z., Hu, Z., Lu, J., Zhou, Z., and Jiao. S. Hexagonal NiS nanobelts as advanced cathode materials for rechargeable Al-ion batteries. *Chem. Commun.* 52: 10427–10430, 2016.

[10] Mohammadi, A.V., Hadjikhani, A., Mohamadi, S.S., and Beidaghi, M. Two-dimensional vanadium carbide (MXene) as a high-capacity cathode material for rechargeable aluminum batteries. *ACS Nano.*, 11: 11135–11144, 2017.

[11] Zhao, Q., Zachman, M. J., Sadat, W. I. Al., Zheng, J., Kourkoutis, L. F., and Archer, L. Solid electrolyte interphases for high-energy aqueous aluminum electrochemical cells. *Sci. Adv.*, 4:8131, 2018.

[12] Wu, C., Gu, S., Zhang, Q., Bai, Y., Li, M., Yuan, Y., Wang, H., Liu, X., Yuan, Y., Zhu, N., Wu, F., Li, H., Gu, L., and Lu, J. Electrochemically activated spinel manganese oxide for rechargeable aqueous aluminum battery. *Nat. Commun.*, 10:73, 2019.

[13] Suo L, Borodin O, Gao T, Olguin M, Ho J, and Fan X et al. "Water-in-salt" electrolyte enables high-voltage aqueous lithium-ion batteries. *Sci.*, 350:938-943, 2015.

[14] Wang, J., Polleux, J., Lim, J., and Dunn, B. Pseudocapacitive contributions to electrochemical energy storage in TiO_2 (Anatase) nanoparticles. *J. Phy. Chem. C*, 111:14925-14931, 2007.